Human Molecular Genetics, 2010, Vol. 19, No. 13 **2682–2694**
doi:10.1093/hmg/ddq158
Advance Access published on April 26, 2010

An accumulation of non-farnesylated prelamin A causes cardiomyopathy but not progeria

Brandon S.J. Davies[1], Richard H. Barnes II[1], Yiping Tu[1], Shuxun Ren[2], Douglas A. Andres[4], H. Peter Spielmann[4], Jan Lammerding[5], Yibin Wang[1,2], Stephen G. Young[1,3] and Loren G. Fong[1,*]

[1]Department of Medicine, [2]Department of Anesthesiology and [3]Department of Human Genetics, David Geffen School of Medicine, University of California, Los Angeles, CA, USA, [4]Department of Molecular and Cellular Biochemistry, University of Kentucky, Lexington, KY, USA and [5]Department of Medicine, Brigham and Women's Hospital/Harvard Medical School, Boston, MA, USA

Received March 16, 2010; Revised and Accepted April 19, 2010

Lamin A is formed from prelamin A by four post-translational processing steps—farnesylation, release of the last three amino acids of the protein, methylation of the farnesylcysteine and the endoproteolytic release of the C-terminal 15 amino acids (including the farnesylcysteine methyl ester). When the final processing step does not occur, a farnesylated and methylated prelamin A accumulates in cells, causing a severe progeroid disease, restrictive dermopathy (RD). Whether RD is caused by the retention of farnesyl lipid on prelamin A, or by the retention of the last 15 amino acids of the protein, is unknown. To address this issue, we created knock-in mice harboring a mutant *Lmna* allele (*Lmna*^{nPLAO}) that yields exclusively non-farnesylated prelamin A (and no lamin C). These mice had no evidence of progeria but succumbed to cardiomyopathy. We suspected that the non-farnesylated prelamin A in the tissues of these mice would be strikingly mislocalized to the nucleoplasm, but this was not the case; most was at the nuclear rim (indistinguishable from the lamin A in wild-type mice). The cardiomyopathy could not be ascribed to an absence of lamin C because mice expressing an otherwise identical knock-in allele yielding only wild-type prelamin A appeared normal. We conclude that lamin C synthesis is dispensable in mice and that the failure to convert prelamin A to mature lamin A causes cardiomyopathy (at least in the absence of lamin C). The latter finding is potentially relevant to the long-term use of protein farnesyltransferase inhibitors, which lead to an accumulation of non-farnesylated prelamin A.

INTRODUCTION

Lamin A, a key component of the nuclear lamina, is formed from a precursor protein, prelamin A, by four enzymatic post-translational processing steps—farnesylation of a cysteine located four amino acids from the C terminus of the protein, endoproteolytic cleavage of the last three amino acids of the protein, carboxyl methylation of the newly exposed farnesylcysteine and endoproteolytic release of the last 15 amino acids of the protein (including the farnesylcysteine methyl ester) (1–5). The last endoproteolytic cleavage step, which releases mature lamin A, is carried out by ZMPSTE24, a membrane zinc metalloproteinase of the endoplasmic reticulum (6–9).

Defects in prelamin A processing and lamin A biogenesis have been linked to progeroid disorders in humans. The classic pediatric progeroid disease, the Hutchinson–Gilford progeria syndrome (HGPS), is caused by a *LMNA* point mutation that alters mRNA splicing, resulting in a 50 amino acid internal deletion in prelamin A (10). This deletion does not affect the C-terminal farnesylation or methylation, but it does remove the site for the last ZMPSTE24 cleavage event. The elimination of the final processing step causes an accumulation of a truncated prelamin A, commonly called progerin,

*To whom correspondence should be addressed at: 695 Charles Young Dr South, Los Angeles, CA 90095, USA. Tel: +1 3102674380; Fax: +1 3102672722; Email: lfong@mednet.ucla.edu

that retains a C-terminal farnesylcysteine methyl ester (11,12). Aside from the farnesylcysteine methyl ester, progerin contains four additional C-terminal residues that are not found in mature lamin A.

Progerin adversely affects the integrity and function of the nuclear lamina, leading to misshapen nuclei in cultured cells and a host of aging-like disease phenotypes (10,13). The frequency of misshapen nuclei in HGPS fibroblasts is reduced with a protein farnesyltransferase inhibitor (FTI) (14–18). Recently, Yang *et al*. (19) generated knock-in mice expressing farnesylated progerin (*Lmna*$^{HG/+}$) and tested whether their progeria-like disease phenotypes might be ameliorated by an FTI. In three independent studies, FTI treatment lessened the severity of disease phenotypes in *Lmna*$^{HG/+}$ mice (19–21). These mouse experiments prompted a clinical trial of FTI therapy in children with HGPS (22).

The favorable results with FTI therapy in *Lmna*$^{HG/+}$ mice have raised hopes for a positive outcome of the FTI trial in humans. However, recent genetic studies in mice have suggested that the FTI treatment strategy may be destined to fall short of a complete cure. Yang *et al*. (12) generated knock-in mice expressing a 'non-farnesylated' version of progerin (*Lmna*$^{nHG/+}$) and showed that those animals developed severe progeria (although somewhat less severe than in mice producing farnesylated progerin). The finding that non-farnesylated progerin elicits disease suggested that an altered primary structure (i.e. the 50 amino acid deletion)—and not merely the farnesyl lipid—contributes to the pathogenesis of HGPS.

A more severe progeroid syndrome, restrictive dermopathy (RD), is caused by a deficiency in ZMPSTE24. ZMPSTE24 deficiency abolishes the final processing step that releases mature lamin A, resulting in an accumulation of a farnesylated and methylated prelamin A. Unlike HGPS, the prelamin A in RD does not have an internal deletion. It does, however, retain the extra 15 amino acids at its C terminus—the segment that is normally absent in mature lamin A.

Currently, no one understands why the accumulation of prelamin A in RD patients (and ZMPSTE24-deficient mice) elicits a progeroid syndrome. One possibility is that disease is largely due to the retention of the farnesyl lipid at the C terminus of prelamin A. However, there are other possibilities. For example, one could reasonably speculate that the extra 15 amino acids at prelamin A's C terminus—and not the lipid anchor—elicit disease. The proposition that an altered primary structure of prelamin A might elicit progeria is not farfetched, given that non-farnesylated progerin causes progeria in mice (12) and given that certain missense mutations in lamins A/C cause progeria in humans (10,23).

In the current study, we tested the hypothesis that the retention of the last 15 amino acids of prelamin A is sufficient to elicit progeria in mice. To approach this issue, we created and analyzed *Lmna* knock-in mice that produce exclusively non-farnesylated prelamin A.

RESULTS

We created *Lmna* knock-in mice expressing exclusively non-farnesylated prelamin A or exclusively wild-type prelamin A. To create a mutant allele yielding only non-farnesylated prelamin A ('non-farnesylated prelamin A-only' allele, *Lmna*^{nPLAO}), we used gene targeting to remove introns 10 and 11 (thereby abolishing lamin C synthesis) and to change the cysteine in the *CaaX* motif to a serine (abolishing protein prenylation; Fig. 1A). To create an allele yielding only wild-type prelamin A ('prelamin A-only' allele, *Lmna*^{PLAO}), we used the same gene-targeting vector except that the cysteine within the *CaaX* motif was not altered (Fig. 1B). Targeted embryonic stem (ES) cell clones (Fig. 1C) were used to create chimeric mice, which were bred to produce heterozygous mice (*Lmna*$^{nPLAO/+}$ and *Lmna*$^{PLAO/+}$). Heterozygotes were then intercrossed to produce homozygotes. *Lmna*$^{nPLAO/+}$ embryonic fibroblasts produced lamin A, lamin C and prelamin A, whereas *Lmna*$^{nPLAO/nPLAO}$ fibroblasts produced exclusively prelamin A (Fig. 1D). Extracts of *Lmna*$^{PLAO/PLAO}$ embryonic fibroblasts contained only mature lamin A (produced from the processing of prelamin A; Fig. 1E). Western blots of extracts from the hearts of *Lmna*$^{nPLAO/nPLAO}$ and *Lmna*$^{PLAO/PLAO}$ mice yielded the expected lamin proteins in the expected amounts (Fig. 1F).

Treatment of fibroblasts with an FTI prevents farnesylation of prelamin A and thus prevents the multistep pathway that converts prelamin A to mature lamin A (12,18). When *Lmna*$^{+/+}$ and *Lmna*$^{PLAO/PLAO}$ fibroblasts were incubated with an FTI, non-farnesylated prelamin A accumulated and was easily detectable by western blotting (i.e. the lamin protein that migrates above mature lamin A; Fig. 2A). The FTI did not affect the migration of the non-farnesylated prelamin A in *Lmna*$^{nPLAO/nPLAO}$ fibroblasts (Fig. 2A). To verify that the prelamin A in *Lmna*$^{nPLAO/nPLAO}$ fibroblasts was not farnesylated, we incubated *Lmna*$^{nPLAO/nPLAO}$ and *Zmpste24*$^{-/-}$ fibroblasts with a farnesol analog, 8-anilinogeraniol (AG) (24). After entering cells, AG is incorporated into anilinogeranyl diphosphate (AGPP), which is used as a substrate by protein farnesyltransferase (FTase) for modifying *CaaX* proteins, including prelamin A. The prelamin A in *Zmpste24*$^{-/-}$ fibroblasts was labeled with AG, and this labeling was largely eliminated with an FTI (Fig. 2B). As expected, there was no AG labeling of the prelamin A in *Lmna*$^{nPLAO/nPLAO}$ fibroblasts, with or without an FTI (Fig. 2B).

In wild-type mouse fibroblasts, lamin A was present at the nuclear rim, but significant amounts were also found in the nucleoplasm (Fig. 3A). Similarly, in *Lmna*$^{PLAO/PLAO}$ fibroblasts, most of lamin A was located at the nuclear rim (Fig. 3A). In *Lmna*$^{nPLAO/nPLAO}$ fibroblasts, some of the prelamin A was at the rim, but substantial amounts were located in the nucleoplasm (Fig. 3A). Also, a higher percentage of the nuclei of *Lmna*$^{nPLAO/nPLAO}$ fibroblasts was misshapen, with blebs and folds ($P < 0.0001$; Fig. 3B and C). Although the nuclei of *Lmna*$^{nPLAO/nPLAO}$ fibroblasts were misshapen, the stiffness of *Lmna*$^{nPLAO/nPLAO}$ nuclei was not significantly different than nuclei of wild-type fibroblasts (Fig. 3D and E).

Immunofluorescence microscopy of tissues from wild-type, *Lmna*$^{PLAO/PLAO}$ and *Lmna*$^{nPLAO/nPLAO}$ mice did not uncover differences in the patterns of lamin A/prelamin A localization. In wild-type and *Lmna*$^{PLAO/PLAO}$ tissues, virtually all the lamin A was at the nuclear rim (Fig. 4). Similarly, virtually all the prelamin A in *Lmna*$^{nPLAO/nPLAO}$ tissues was located at the nuclear rim (Fig. 4).

Body weight curves in male *Lmna*$^{+/+}$, *Lmna*$^{PLAO/PLAO}$ and *Lmna*$^{nPLAO/nPLAO}$ mice were not significantly different

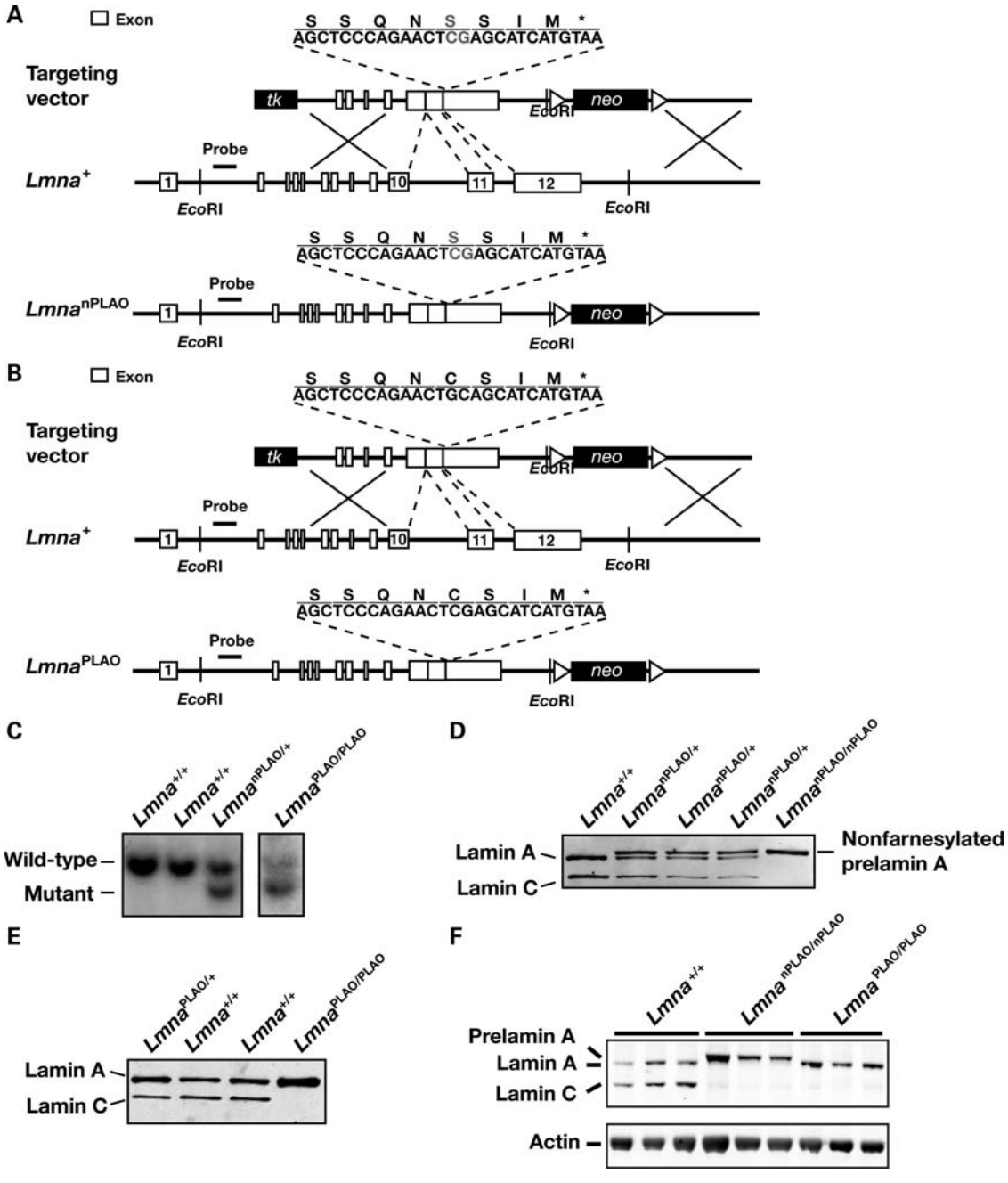

Figure 1. Production of knock-in mice that express a non-farnesylated version of prelamin A or wild-type prelamin A. (**A**) Gene-targeting strategy to create a mutant *Lmna* allele, $Lmna^{nPLAO}$, that yields exclusively a non-farnesylated version of prelamin A. This vector removes introns 10 and 11 (thereby abolishing synthesis of lamin C) and introduces a point mutation that changes the cysteine in the *CaaX* motif to a serine (thereby abolishing protein prenylation). (**B**) Gene-targeting strategy to create a mutant *Lmna* allele, $Lmna^{PLAO}$, that yields exclusively wild-type prelamin A. This vector removes introns 10 and 11 but leaves the *CaaX* motif intact. (**C**) Southern blot identification of targeting events in ES cell clones. The genomic DNA was cleaved with *Eco*RI, and the blot was hybridized with the indicated 5′ flanking probe. (**D**) Western blot of $Lmna^{+/+}$, $Lmna^{nPLAO/+}$ and $Lmna^{nPLAO/nPLAO}$ fibroblasts with a lamin A/C-specific antibody. (**E**) Western blot of $Lmna^{+/+}$, $Lmna^{PLAO/+}$ and $Lmna^{PLAO/PLAO}$ fibroblasts with a lamin A/C-specific antibody. (**F**) A western blot, with an antibody against lamin A/C, showing prelamin A, lamin A and lamin C in the hearts of $Lmna^{+/+}$, $Lmna^{nPLAO/nPLAO}$ and $Lmna^{PLAO/PLAO}$ mice ($n = 3$ mice/genotype). Actin levels were measured as a loading control.

(Fig. 5A), but female $Lmna^{PLAO/PLAO}$ and $Lmna^{nPLAO/nPLAO}$ mice appeared to have slightly lower body weights than $Lmna^{+/+}$ littermates (Fig. 5B). The survival of $Lmna^{PLAO/PLAO}$ mice was not different than that of wild-type mice. Male and female $Lmna^{nPLAO/nPLAO}$ mice appeared to be entirely normal for the first 20 weeks of life. After that, however, we observed premature death in males and females; all male $Lmna^{nPLAO/nPLAO}$ mice succumbed by 44 weeks of age (median survival, 38.5 weeks) and all female mice succumbed by 80 weeks (median survival, 49.5 weeks). Kaplan–Meier survival analysis revealed that the survival of $Lmna^{nPLAO/nPLAO}$ mice was significantly reduced, compared with $Lmna^{+/+}$ or

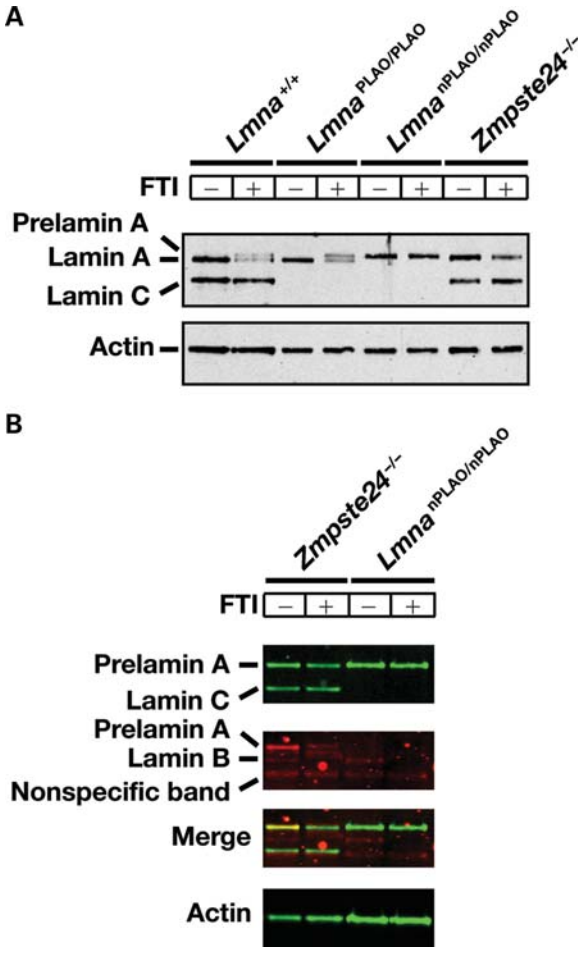

Figure 2. Prelamin A processing in *Lmna*$^{PLAO/PLAO}$ and *Lmna*$^{nPLAO/nPLAO}$ fibroblasts. (**A**) Western blots, with an antibody against lamin A/C, showing lamin A, prelamin A and lamin C in *Lmna*$^{+/+}$, *Lmna*$^{PLAO/PLAO}$, *Lmna*$^{nPLAO/nPLAO}$ and *Zmpste24*$^{-/-}$ fibroblasts in the presence and the absence of an FTI (ABT-100; 5 μM). Actin was used as a loading control. (**B**) Metabolic labeling experiment with a farnesol analog, AG to assess the farnesylation of prelamin A. Fibroblasts were incubated with AG (50 μM) in the presence (+) or the absence (−) of an FTI (ABT-100, 5 μM). Western blots were performed on cell extracts with an antibody specific for lamin A/C (green) and an antibody specific for AG (red). As expected, the FTI blocked the incorporation of AG into the prelamin A in *Zmpste24*$^{-/-}$ fibroblasts. No farnesylation of prelamin A in *Lmna*$^{nPLAO/nPLAO}$ cells was detected. In the AG western blot, lamin B1 was detected (electrophoretic mobility intermediate between lamin A and lamin C); this band disappeared with an FTI. A non-specific band was also observed in the AG western blot (electrophoretic band immediately beneath lamin C).

Lmna$^{PLAO/PLAO}$ mice ($P < 0.0001$ for both males and females; Fig. 5C and D).

The premature death in *Lmna*$^{nPLAO/nPLAO}$ mice suggested that non-farnesylated prelamin A might elicit cardiomyopathy. Indeed, echocardiography revealed that *Lmna*$^{nPLAO/nPLAO}$ mice had a dilated cardiomyopathy (Fig. 6A and B), with an increased left ventricular (LV) chamber size during systole (Fig. 6C) and a reduced LV ejection fraction (Fig. 6D). In keeping with these findings, the expression of myosin heavy chain alpha (*Myh6*), which typically falls in the setting of cardiomyopathy (25), was reduced in *Lmna*$^{nPLAO/nPLAO}$ mice (Fig. 6E). The expression of myosin heavy chain beta (*Myh7*), a marker of cardiomyopathy (25), was increased in *Lmna*$^{nPLAO/nPLAO}$ mice (Fig. 6F). This cardiomyopathy phenotype, with a greater severity in males, is similar to the phenotype of *Lmna* knock-in mice carrying an H222P substitution (26). *Lmna*$^{H222P/H222P}$ mice were reported to have a 'marked increase in fibrosis' in the left and right ventricles. We examined cardiac pathology in an *Lmna*$^{nPLAO/nPLAO}$ mouse that had severe cardiomyopathy by echocardiography and found significant fibrosis in the papillary muscle of the left ventricle, as judged by a Gomori trichrome stain (Fig. 7). No such fibrosis was observed in the papillary muscle of an age-matched *Lmna*$^{+/+}$ control mouse (Fig. 7). We would characterize the fibrosis in the *Lmna*$^{nPLAO/nPLAO}$ mouse as being mild–moderate, and in some mice, fibrosis was minimal.

In humans, lamin-related progeroid syndromes are associated with osteolytic lesions in bones, a severe growth defect, and reduced survival (10,27,28). *Zmpste24*$^{-/-}$ mice share these phenotypes. Indeed, osteolytic lesions and spontaneous rib fractures are prominent in *Zmpste24*$^{-/-}$ mice, which accumulate the farnesylated form of prelamin A (Fig. 8). Interestingly, *Lmna*$^{nPLAO/nPLAO}$ mice did not have osteolytic lesions in any of their bones, and rib fractures were never observed (Fig. 8). Bone lesions were also absent in *Lmna*$^{PLAO/PLAO}$ mice (Fig. 8). *Zmpste24*$^{-/-}$ and *Lmna*$^{nPLAO/nPLAO}$ mice also differed in their body weight curves. *Zmpste24*$^{-/-}$ mice were far smaller than wild-type mice, and they invariably die from severe, progressive inanition (6,8,9; also see Fig. 9). At 5–6 months of age, *Zmpste24*$^{-/-}$ mice typically weigh only 11–17 g (6,8,9; also see Fig. 9), whereas 5–6-month-old *Lmna*$^{nPLAO/nPLAO}$ typically weigh 30–40 g (Fig. 5). Thus, the non-farnesylated prelamin A in *Lmna*$^{nPLAO/nPLAO}$ mice elicits none of the progeria-like disease phenotypes found in *Zmpste24*$^{-/-}$ mice, but it does cause cardiomyopathy.

The *Lmna*^{PLAO} allele yields exclusively prelamin A, whereas a wild-type *Lmna* allele yields both lamin C and prelamin A. Because all of the output of the *Lmna*^{PLAO} allele is channeled into prelamin A production, we predicted that the *Lmna*^{PLAO} allele would increase prelamin A levels in *Zmpste24*$^{-/-}$ mice and worsen disease phenotypes. Indeed, this was the case. Prelamin A levels increased with each additional *Lmna*^{PLAO} allele (Fig. 9A and B), and both body weight and survival worsened (Fig. 9C and D).

DISCUSSION

Finding progeria-like disease phenotypes in 'non-farnesylated progerin mice' (12) was intriguing because it suggested that the primary structure of progerin, and not merely its farnesyl lipid anchor, could be central to the pathogenesis of HGPS. Those findings immediately raised parallel questions about the pathogenesis of RD (ZMPSTE24 deficiency). When ZMPSTE24 is absent, are the disease phenotypes elicited by the retention of the hydrophobic lipid anchor on prelamin A or are they due to the extra 15 amino acids at the protein's C terminus? To address this issue, we created 'knock-in mice' (*Lmna*$^{nPLAO/nPLAO}$) that synthesize exclusively non-farnesylated prelamin A. Given the unequivocal findings with 'non-farnesylated progerin mice', we hypothesized that

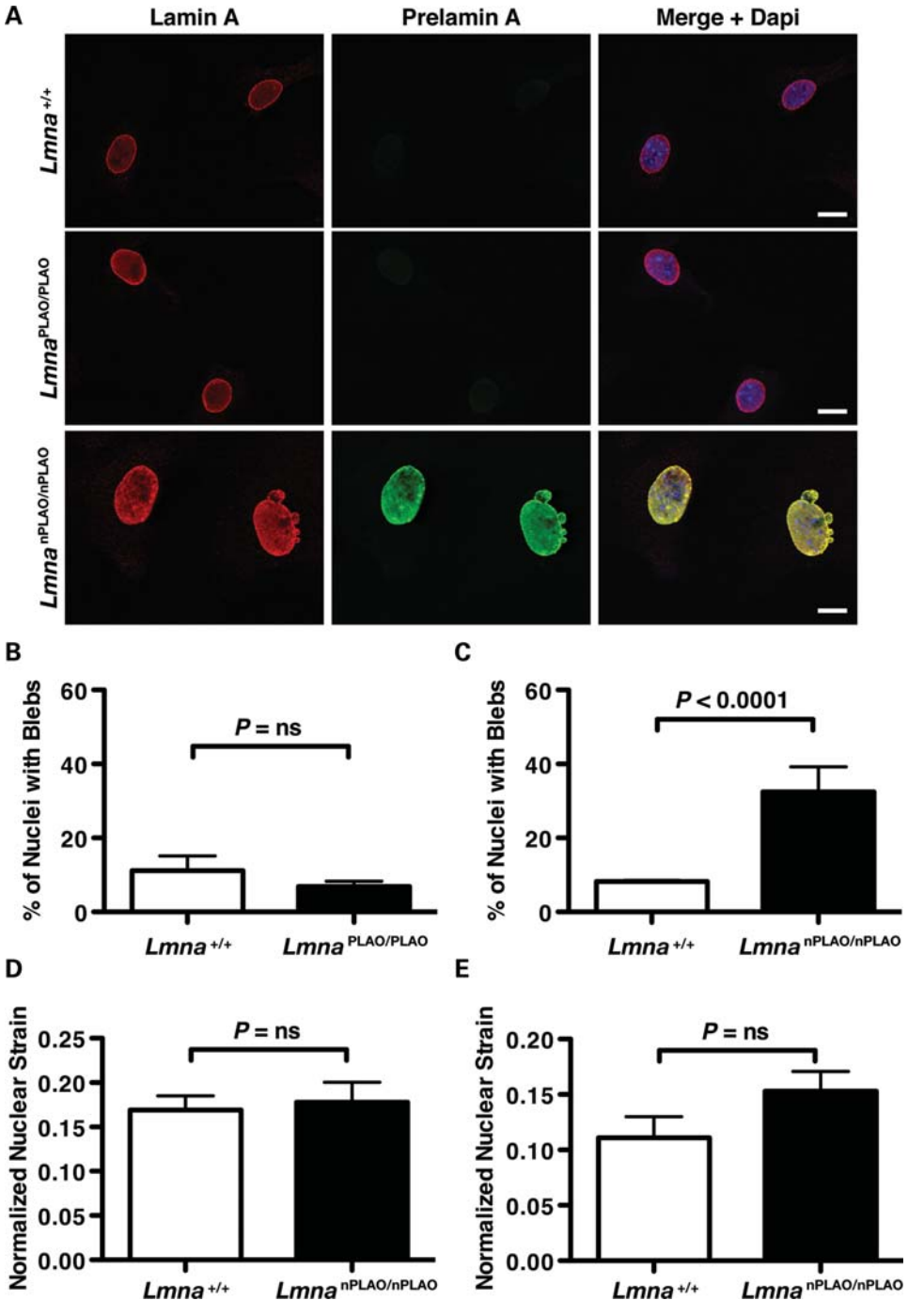

Figure 3. Phenotypes of fibroblasts from *Lmna*$^{PLAO/PLAO}$ and *Lmna*$^{nPLAO/nPLAO}$ mice. (**A**) Immunostaining of fibroblasts from *Lmna*$^{+/+}$, *Lmna*$^{PLAO/PLAO}$ and *Lmna*$^{nPLAO/nPLAO}$ mice with lamin A-specific (red) and prelamin A-specific (green) antibodies (clone 3C8). Nuclei were counterstained with DAPI (blue). Images were taken with a confocal microscope. Scale bars represent 15 μm. Bar graphs showing the percentage of nuclei with blebs in *Lmna*$^{PLAO/PLAO}$ (**B**) and *Lmna*$^{nPLAO/nPLAO}$ (**C**) fibroblasts compared with *Lmna*$^{+/+}$ control cells. (**D** and **E**) Analysis of nuclear stiffness in *Lmna*$^{+/+}$ and *Lmna*$^{nPLAO/nPLAO}$ fibroblasts. We examined fibroblasts that had been immortalized by repeated passaging (D) and also low-passage number primary embryonic fibroblasts (E). In both cases, we observed no significant difference in nuclear deformation under uniaxial strain application, compared with *Lmna*$^{+/+}$ cells. The extent of nuclear deformations was measured and is expressed as a ratio of nuclear strain to applied membrane strain (normalized nuclear strain).

the 'non-farnesylated prelamin A mice' would manifest all the same progeria-like disease phenotypes found in *Zmpste24*$^{-/-}$ mice. To our surprise, this hypothesis was proven wrong. Even though *Lmna*$^{nPLAO/nPLAO}$ mice expressed very high levels of non-farnesylated prelamin A, they bore no resemblance to *Zmpste24*$^{-/-}$ mice. Unlike *Zmpste24*$^{-/-}$ mice, *Lmna*$^{nPLAO/nPLAO}$ mice maintained a normal or near-normal body weight, and they had no osteolytic lesions or bone fractures. In contrast to the *Zmpste24*$^{-/-}$ mice, *Lmna*$^{nPLAO/nPLAO}$ mice did develop a dilated cardiomyopathy. The most

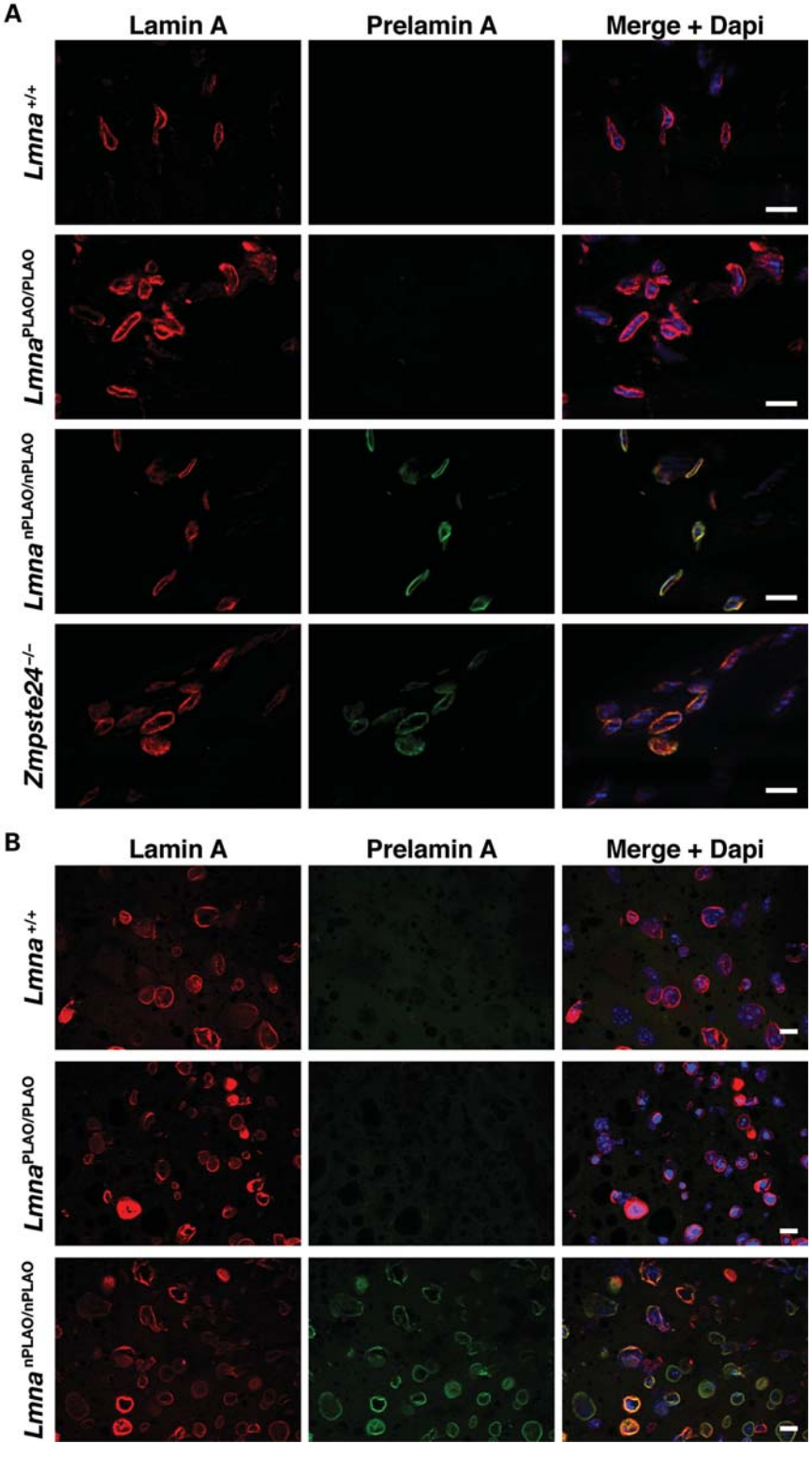

Figure 4. Nuclear rim localization of lamin A and prelamin A in tissues of *Lmna*$^{PLAO/PLAO}$ and *Lmna*$^{nPLAO/nPLAO}$ mice. (**A**) Immunostaining of heart from *Lmna*$^{+/+}$, *Lmna*$^{PLAO/PLAO}$, *Lmna*$^{nPLAO/nPLAO}$ and *Zmpste24*$^{-/-}$ mice with lamin A-specific (red) and prelamin A-specific (clone 3C8; green) antibodies. Nuclei were counterstained with DAPI (blue). Scale bars represent 20 μm. (**B**) Immunostaining of liver from *Lmna*$^{+/+}$, *Lmna*$^{PLAO/PLAO}$ and *Lmna*$^{nPLAO/nPLAO}$ mice with lamin A-specific (red) and prelamin A-specific (clone 7G11; green) antibodies. Nuclei were counterstained with DAPI (blue). Scale bars represent 20 μm.

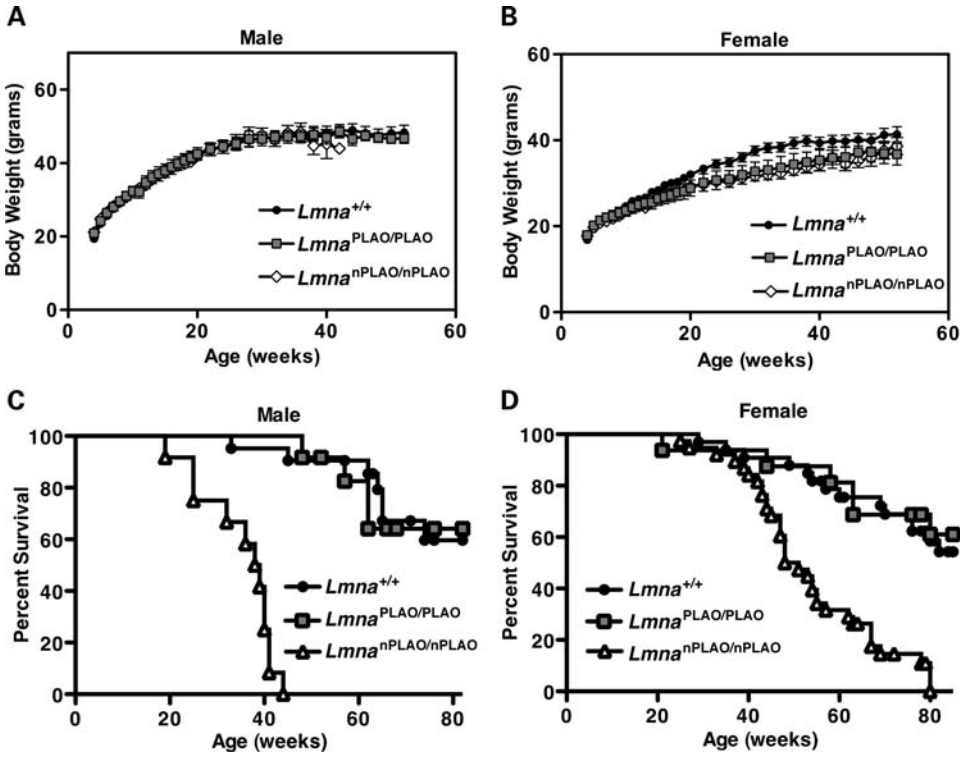

Figure 5. Body weight and survival curves for $Lmna^{PLAO/PLAO}$ and $Lmna^{nPLAO/nPLAO}$ mice. (**A**) Body weight curves for male $Lmna^{+/+}$ ($n = 27$), $Lmna^{PLAO/PLAO}$ ($n = 12$) and $Lmna^{nPLAO/nPLAO}$ mice ($n = 20$). (**B**) Body weight curves for female $Lmna^{+/+}$ ($n = 28$), $Lmna^{PLAO/PLAO}$ ($n = 12$) and $Lmna^{nPLAO/nPLAO}$ mice ($n = 22$). Body weights of female $Lmna^{PLAO/PLAO}$ and $Lmna^{nPLAO/nPLAO}$ mice were slightly lower than those of $Lmna^{+/+}$ mice ($P < 0.001$). (**C**) Kaplan–Meier survival plots for male $Lmna^{+/+}$ ($n = 21$), $Lmna^{PLAO/PLAO}$ ($n = 12$) and $Lmna^{nPLAO/nPLAO}$ mice ($n = 12$). Survival time for male $Lmna^{nPLAO/nPLAO}$ mice was shorter than for $Lmna^{+/+}$ or $Lmna^{PLAO/PLAO}$ mice ($P < 0.0001$). (**D**) Kaplan–Meier survival plots for female $Lmna^{+/+}$ ($n = 33$), $Lmna^{PLAO/PLAO}$ ($n = 16$) and $Lmna^{nPLAO/nPLAO}$ mice ($n = 38$). Survival time for female $Lmna^{nPLAO/nPLAO}$ mice was shorter than that for $Lmna^{+/+}$ or $Lmna^{PLAO/PLAO}$ mice ($P < 0.0001$).

parsimonious interpretation of our findings is that the lipid anchor on prelamin A is central to disease phenotypes in $Zmpste24^{-/-}$ mice, whereas the extra 15 amino acid residues at the end of prelamin A are not. In addition, we conclude that non-farnesylated prelamin A leads to a distinct disease phenotype, dilated cardiomyopathy, which is not found in $Zmpste24^{-/-}$ mice. Clearly, non-farnesylated prelamin A is not functionally equivalent to mature lamin A.

The involvement of *Lmna* in cardiomyopathy is not without precedent. In humans, many *LMNA* missense mutations cause muscular dystrophy and/or dilated cardiomyopathy with conduction system disease (29–31). Several of the missense mutations observed in humans have been introduced into mouse *Lmna*, and homozygous mice for those mutations manifest cardiomyopathy and premature death (26,32). The available data suggest that lamin A/C-related cardiomyopathy could be caused by increased nuclear fragility and changes in gene expression, in particular the MAPK pathway (33). Interestingly, no one has yet found a case of cardiomyopathy due to a missense mutation involving the last 15 amino acids of prelamin A, nor has anyone identified a *CaaX* motif mutation leading to the production of non-farnesylated prelamin A.

The conclusion that non-farnesylated prelamin A leads to cardiomyopathy, but not progeria, is subject to several caveats. First, we would point out that $Lmna^{nPLAO/nPLAO}$ mice are incapable of producing lamin C. Thus, one could conceivably postulate that the cardiomyopathy is elicited by the inability to make that lamin isoform. However, this explanation seems unlikely, given the complete absence of cardiomyopathy or decreased survival in $Lmna^{PLAO/PLAO}$ mice (which also cannot make lamin C). It remains a formal possibility that cardiomyopathy is caused by non-farnesylated prelamin A, but only in the absence of lamin C. Second, it is important to note that prelamin A farnesylation was eliminated in $Lmna^{nPLAO/nPLAO}$ mice by introducing a cysteine-to-serine substitution in prelamin A's *CaaX* motif. That amino acid substitution is remarkably subtle, amounting to replacing a single sulfur atom with an oxygen atom. Nevertheless, one could propose that this amino acid substitution is solely responsible for the cardiomyopathy. Against that idea, however, is the absence of cardiomyopathy in 'non-farnesylated progerin mice' (12), which share the identical cysteine-to-serine substitution in the *CaaX* motif.

The ideal scenario would be to create 'non-farnesylated prelamin A mice' without introducing any mutation into prelamin A's *CaaX* motif. Unfortunately, we are not aware of any strategy that would make this possible. In theory, one could achieve this goal by eliminating the expression of FTase, a genetic intervention that would lead to the accumulation of non-farnesylated prelamin A (34). For such an approach to be practical, however, FTase deficiency could not elicit any of its own

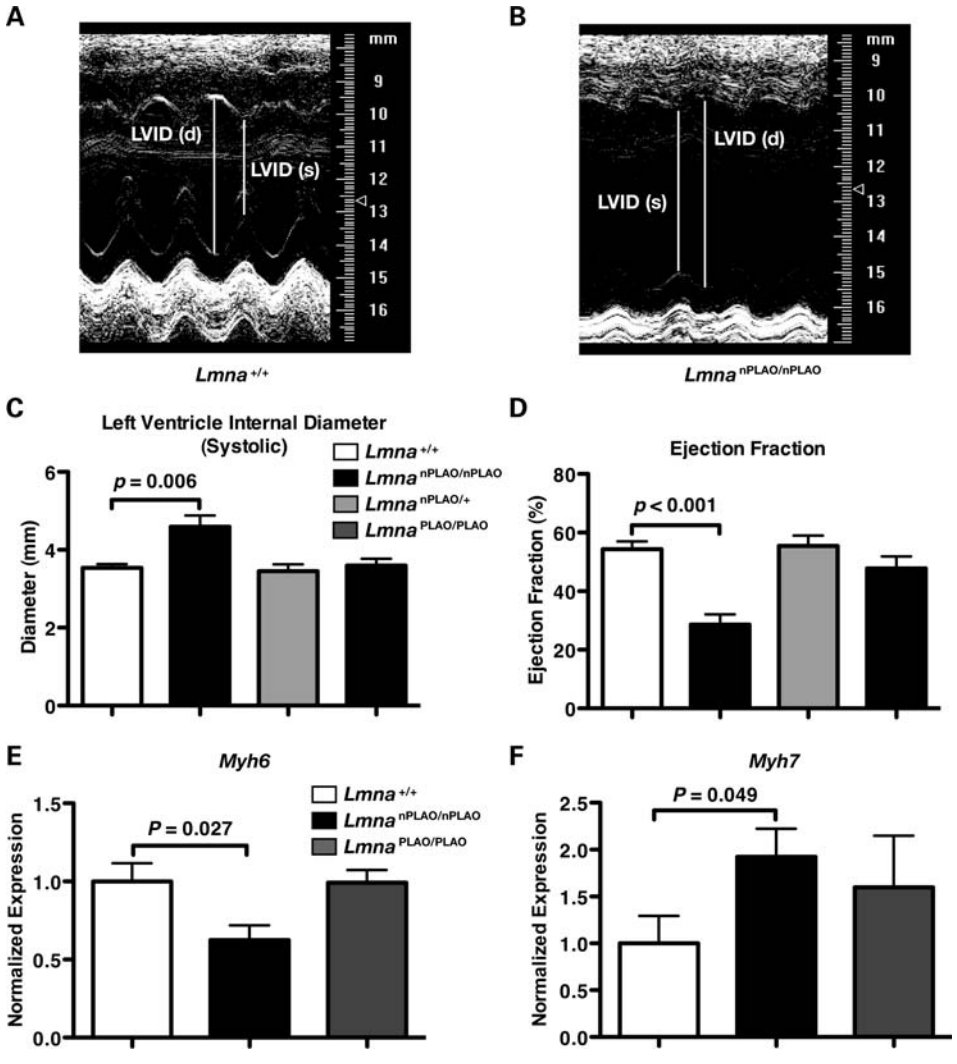

Figure 6. Dilated cardiomyopathy in *Lmna*$^{nPLAO/nPLAO}$ mice. Representative *M*-mode echocardiograms of *Lmna*$^{+/+}$ (**A**) and *Lmna*$^{nPLAO/nPLAO}$ (**B**) mice. Lines depict the systolic (s) and diastolic (d) LV internal diameters (LVIDs). Quantification of systolic LVID (**C**) and LV ejection fraction (**D**) in *Lmna*$^{+/+}$, *Lmna*$^{nPLAO/nPLAO}$, *Lmna*$^{nPLAO/+}$ and *Lmna*$^{PLAO/PLAO}$ mice ($n = 6$/genotype). Bar graphs show mean ± SEM. *Myh6* (**E**) and *Myh7* (**F**) expression levels in the hearts of *Lmna*$^{+/+}$, *Lmna*$^{nPLAO/nPLAO}$ and *Lmna*$^{PLAO/PLAO}$ mice ($n = 7$/genotype). Expression levels were measured by quantitative RT–PCR and normalized to *Gapdh* (mean ± SEM).

untoward consequences. Unfortunately, this is not the case. FTase has >60 protein substrates (35,36), and a deficiency in this enzyme elicits pathology in multiple cell types. A complete deficiency of FTase causes early embryonic lethality (37). Although initially reported that a knockout of FTase in adult mice leads to little if any pathology (37), it is now clear that this is not the case. FTase deficiency in skin keratinocytes yields severe alopecia (34), and an absence of FTase in liver causes severe hepatocellular disease (Shao H. Yang, unpublished observations). Thus, an attempt to produce 'non-farnesylated prelamin A mice' by eliminating FTase expression would be fraught with significant complications.

The absence of disease phenotypes in *Lmna*$^{PLAO/PLAO}$ mice implies that lamin C synthesis is dispensable in the laboratory mouse. In earlier studies, Fong *et al*. (38) found no disease phenotypes in mice synthesizing exclusively lamin C (*Lmna*$^{LCO/LCO}$), leading them to conclude that lamin A synthesis is dispensable. An absence of 'both' lamin A and lamin C causes muscular dystrophy and cardiomyopathy (39). Thus, a key lesson from the *Lmna*$^{PLAO/PLAO}$ and *Lmna*$^{LCO/LCO}$ models is that lamin A alone, or lamin C alone, is capable of preventing disease. Also, when we state that each isoform is 'dispensable', we simply mean only that an absence of one isoform does not lead to obvious disease. In the future, it is conceivable that newer and more sensitive assays could uncover unique and important physiologic roles for each of the two protein isoforms.

Dogma has held that prelamin A's hydrophobic lipid anchor is important for the targeting of the protein to the inner nuclear membrane (which is adjacent to the nuclear lamina). In part, this conclusion rested on the observation that prelamin A appears in the nucleoplasm of cultured fibroblasts, rather than at the nuclear rim, when protein farnesylation is inhibited (40). Also, two groups reported that when a 'non-farnesylated prelamin A construct' was transfected into cells, the prelamin A did not reach the nuclear rim (5,41). A third study found that some non-farnesylated prelamin A reached the nuclear rim,

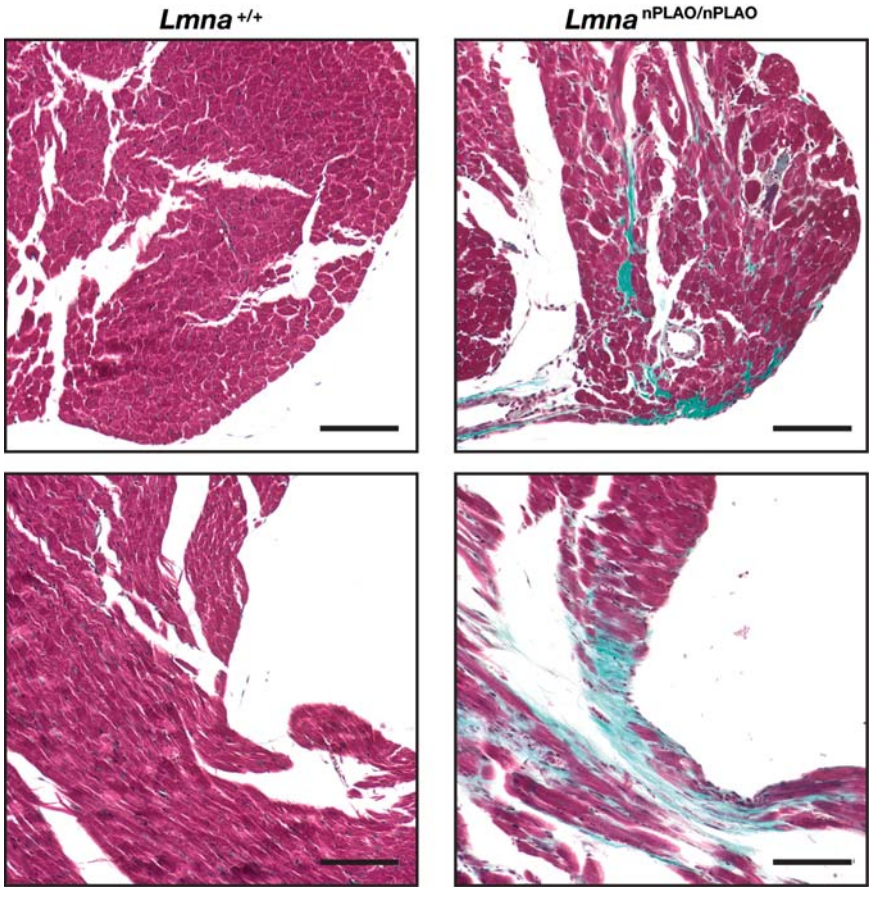

Figure 7. Fibrosis within an LV papillary muscle from a male *Lmna*$^{nPLAO/nPLAO}$ mouse, as judged by a Gomori trichrome stain. This *Lmna*$^{nPLAO/nPLAO}$ mouse had severe LV dysfunction, as judged by echocardiography. Fibrotic tissue is stained green. No papillary muscle fibrosis was observed in an age- and sex-matched littermate *Lmna*$^{+/+}$ mouse. Scale bars represent 100 μm.

but with delayed kinetics (42). Recently, however, the conclusion that farnesylation is important for the nuclear envelope targeting of prelamin A has been challenged. Lamin C, which is never farnesylated, reaches the nuclear rim, even in the absence of lamin A, suggesting that farnesylation is not a requirement for nuclear rim localization of that nuclear lamin (38). Lee *et al*. (34) generated keratinocyte-specific FTase knockout mice and showed that FTase-deficient keratinocytes accumulate substantial amounts of non-farnesylated prelamin A. Taking advantage of a new monoclonal antibody against mouse prelamin A, Lee *et al*. (34) showed that the non-farnesylated prelamin A in FTase-deficient keratinocytes is located largely or exclusively at the nuclear rim, indistinguishable from the localization of mature lamin A in wild-type keratinocytes. Little if any non-farnesylated prelamin A was found in the nucleoplasm. In the current study, we observed consistent findings. As judged by immunofluorescence microscopy, virtually all of the non-farnesylated prelamin A in the heart and liver of *Lmna*$^{nPLAO/nPLAO}$ mice was located at the nuclear rim. Indeed, the distribution of non-farnesylated prelamin A in those tissues was identical to the distribution of mature lamin A in *Lmna*$^{PLAO/PLAO}$ tissues. Thus, prelamin A's farnesyl lipid anchor is not required for targeting to the nuclear rim. In *Lmna*$^{nPLAO/nPLAO}$ fibroblasts, non-farnesylated prelamin A was also found at the nuclear rim, although the amount was somewhat less than the amount of mature lamin A at the nuclear rim in wild-type fibroblasts.

Several years ago, Fong *et al*. (8,38) showed that the disease phenotypes in *Zmpste24*$^{-/-}$ mice could be eliminated by reducing farnesyl-prelamin A production, either by introducing an *Lmna* knockout allele or an *Lmna*^{LCO} allele (an allele yielding exclusively lamin C). Those findings supported the concept that farnesyl-prelamin A is toxic and provided the first suggestion that strategies to reduce prelamin A production could be therapeutically useful in progeria. The current studies with the *Lmna*^{PLAO} allele further underscore the toxicity of farnesyl-prelamin A. Because the *Lmna*^{PLAO} allele yields exclusively prelamin A, *Zmpste24*$^{-/-}$ mice harboring that allele synthesize increased amounts of farnesyl-prelamin A. Larger amounts of farnesyl-prelamin A clearly lead to more toxicity: the disease phenotypes in *Zmpste24*$^{-/-}$*Lmna*$^{PLAO/PLAO}$ mice were far more severe than those in *Zmpste24*$^{-/-}$*Lmna*$^{PLAO/+}$ mice, which in turn were more severe than those in *Zmpste24*$^{-/-}$*Lmna*$^{+/+}$ mice.

From the standpoint of therapy, the current study would suggest that an FTI has the potential to be a double-edged sword. On the one hand, our findings suggest that reducing protein farnesylation with an FTI might be useful, in that non-farnesylated prelamin A appears to be devoid of the capacity to elicit progeria-like disease phenotypes. That conclusion is consistent with an earlier study showing that an FTI

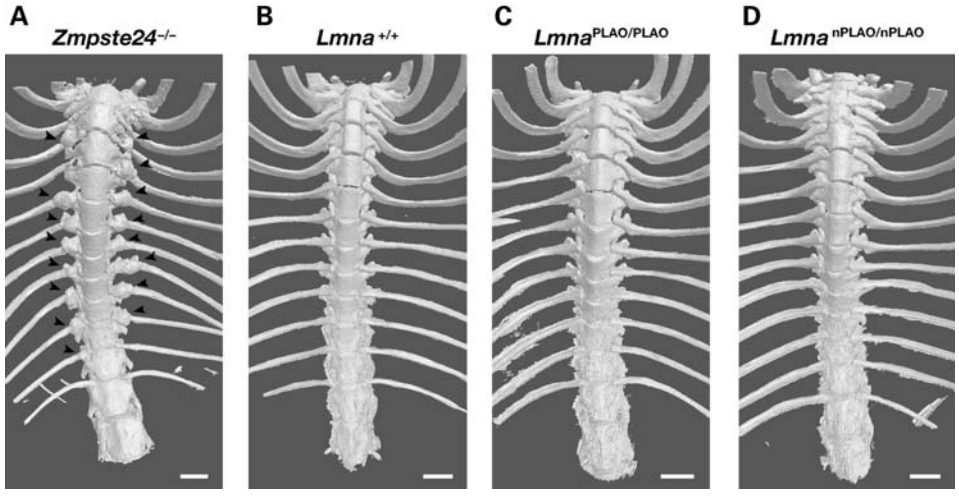

Figure 8. Surface renderings of μCT scans showing the lack of bone abnormalities in *Lmna*$^{PLAO/PLAO}$ and *Lmna*$^{nPLAO/nPLAO}$ mice. (**A**) Scans showing characteristic rib fractures in 7-month-old *Zmpste24*$^{-/-}$ mice. Arrowheads indicate rib fractures and surrounding callus. No rib fractures were observed in *Lmna*$^{+/+}$ (**B**), *Lmna*$^{PLAO/PLAO}$ (**C**) or *Lmna*$^{nPLAO/nPLAO}$ (**D**) mice. Scale bars represent 2.5 mm.

ameliorates disease in *Zmpste24*$^{-/-}$ mice (43). On the other hand, our studies offer a darker possibility—that non-farnesylated prelamin A carries its own distinctive toxicity, dilated cardiomyopathy. Thus, it is theoretically possible that any accumulation of non-farnesylated prelamin A, such as would occur with a long-term FTI therapy, could adversely affect the heart. Fortunately, we are not aware of any reports of cardiomyopathy with FTI therapy in humans, nor have we observed any evidence of cardiomyopathy when treating mice with an FTI, but any physician contemplating long-term FTI treatment for progeroid disorders should be attuned to this possibility.

MATERIALS AND METHODS

Generation of knock-in mice

To create a mutant *Lmna* allele yielding only non-farnesylated prelamin A (*Lmna*^{nPLAO}), we used a gene-targeting vector similar to one used to create a mutant allele yielding exclusively progerin (*Lmna*^{HG}) (18). Introns 10 and 11 of *Lmna* were deleted by site-directed mutagenesis (QuikChange; Stratagene, La Jolla, CA, USA). The oligonucleotide 5′-GATG GAGAAGAGCTCCTCCATCACCACCGTGGTTCCCACTG CAGCGGCTCGGGGGACCCC-3′ and its reverse complement were used to delete intron 10; oligonucleotide 5′-CT CCTGGGCAACTCCAGTCCCCGGAGCCAGAGCTCCCA GAACTGCAGCATCATGTAATCT-3′ and its reverse complement were used to delete intron 11. Also, a point mutation was introduced into exon 12 that changes the cysteine of prelamin A's *CaaX* motif to a serine (i.e. −CSIM to −SSIM). The mutation was introduced into the 5′ arm of the vector by site-directed mutagenesis with the QuikChange kit (Stratagene) and oligonucleotide 5′-CAGAGCTCCCAGAA CTCGAGCATCATGTAATCT-3′ (and the complementary primer). To create a mutant *Lmna* allele yielding only wild-type prelamin A (*Lmna*^{PLAO}), the same gene-targeting vector was used, except that the *CaaX* motif was not changed. The integrity of both gene-targeting vectors was verified by restriction endonuclease digestion and DNA sequencing.

Gene-targeting vectors were linearized with *Not*I and electroporated into 129/OlaHsd mouse ES cells. Targeted clones were identified by Southern blotting with *Eco*RI-cleaved genomic DNA with a 348 bp 5′ flanking probe (12). Targeted ES cells were microinjected into C57BL/6 blastocysts, and the resulting chimeras were bred with C57BL/6 females to generate *Lmna*$^{PLAO/+}$ and *Lmna*$^{nPLAO/+}$ mice. Heterozygous mice were intercrossed to generate homozygous mice (*Lmna*$^{PLAO/PLAO}$ and *Lmna*$^{nPLAO/nPLAO}$). *Lmna*$^{PLAO/+}$ mice were also bred with *Zmpste24*$^{+/-}$ mice (44) and their offspring intercrossed to obtain *Lmna*$^{+/+}$*Zmpste24*$^{+/+}$, *Lmna*$^{PLAO/PLAO}$*Zmpste24*$^{+/+}$, *Lmna*$^{+/+}$*Zmpste24*$^{-/-}$, *Lmna*$^{PLAO/+}$*Zmpste24*$^{-/-}$ and *Lmna*$^{PLAO/PLAO}$*Zmpste24*$^{-/-}$ mice. Genotyping of mice was performed by PCR using DNA from tail biopsies (18). All mice were fed a chow diet and housed in a virus-free barrier facility with a 12 h light–dark cycle. All mouse experiments were approved by UCLA's Animal Research Committee.

Western blots and metabolic labeling

Primary mouse embryonic fibroblasts were prepared from embryonic day 13.5 embryos (6). To block protein farnesylation, we added a highly selective FTI, ABT-100 (5 μM), to the cell culture medium.

Urea-soluble extracts were prepared as described previously (45). Extracts were size-fractionated on 4–12% gradient polyacrylamide Bis–Tris gels (Invitrogen), and the separated proteins transferred to nitrocellulose membranes for western blotting. Antibody dilutions were 1:200 for anti-lamin A/C goat IgG (sc-6215, Santa Cruz Biotechnology), 1:1000 for anti-actin goat IgG (sc-1616, Santa Cruz Biotechnology) and 1:5000 for IRDye 800 anti-goat IgG (Rockland Immunochemicals). The IR-coupled antibodies were detected with an Odyssey infrared imaging scanner and quantified according to the manufacturer's instructions.

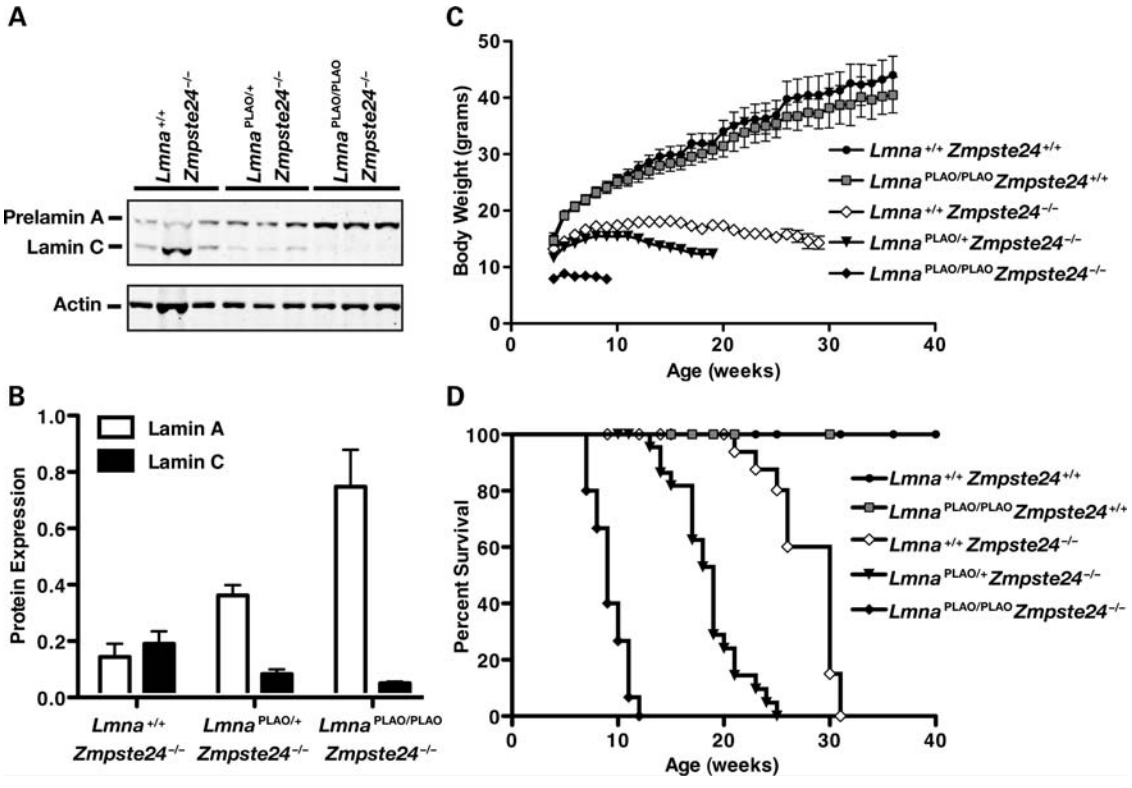

Figure 9. The *Lmna*^{PLAO} allele worsens the progeria-like disease phenotypes in *Zmpste24*$^{-/-}$ mice in a dose-dependent manner. (**A**) Western blots (with an antibody against lamin A/C) showing prelamin A and lamin C in the kidneys of *Lmna*$^{+/+}$*Zmpste24*$^{-/-}$, *Lmna*$^{PLAO/+}$*Zmpste24*$^{-/-}$ and *Lmna*$^{PLAO/PLAO}$*Zmpste24*$^{-/-}$ mice ($n = 3$/genotype). (**B**) Quantitative analysis of prelamin A and lamin C expression in the kidney in *Lmna*$^{+/+}$*Zmpste24*$^{-/-}$, *Lmna*$^{PLAO/+}$*Zmpste24*$^{-/-}$ and *Lmna*$^{PLAO/PLAO}$*Zmpste24*$^{-/-}$ mice (bar graphs depict prelamin A:actin and lamin C:actin ratios). (**C**) Body weight curves for *Lmna*$^{+/+}$*Zmpste24*$^{+/+}$ ($n = 25$), *Lmna*$^{PLAO/PLAO}$*Zmpste24*$^{+/+}$ ($n = 17$), *Lmna*$^{+/+}$*Zmpste24*$^{-/-}$ ($n = 24$), *Lmna*$^{PLAO/+}$*Zmpste24*$^{-/-}$ ($n = 24$) and *Lmna*$^{PLAO/PLAO}$*Zmpste24*$^{-/-}$ ($n = 15$) mice. Body weight curves for *Lmna*$^{+/+}$*Zmpste24*$^{+/+}$ and *Lmna*$^{PLAO/PLAO}$*Zmpste24*$^{+/+}$ mice were not significantly different. Body weight curves for all other genotypes were significantly different from wild-type mice and from each other ($P < 0.01$ between *Lmna*$^{+/+}$*Zmpste24*$^{-/-}$ and *Lmna*$^{PLAO/+}$*Zmpste24*$^{-/-}$ mice; $P < 0.001$ for all other comparisons). (**D**) Kaplan–Meier survival plots for *Lmna*$^{+/+}$*Zmpste24*$^{+/+}$ ($n = 26$), *Lmna*$^{PLAO/PLAO}$*Zmpste24*$^{+/+}$ ($n = 16$), *Lmna*$^{+/+}$*Zmpste24*$^{-/-}$ ($n = 23$), *Lmna*$^{PLAO/+}$*Zmpste24*$^{-/-}$ ($n = 24$) and *Lmna*$^{PLAO/PLAO}$*Zmpste24*$^{-/-}$ ($n = 15$) mice. Survival times for *Lmna*$^{+/+}$*Zmpste24*$^{+/+}$ and *Lmna*$^{PLAO/PLAO}$*Zmpste24*$^{+/+}$ mice were not statistically different. Survival times for all other genotypes were significantly different from the wild-type mice and from each other ($P < 0.001$ for all comparisons).

To assess protein farnesylation, fibroblasts were incubated for 48 h with an analog of farnesol, AG (50 μM in DMSO) (24). AG is incorporated into AGPP and used as a substrate by protein farnesyltransferase. The incorporation of AG into CaaX proteins such as prelamin A can be detected by western blotting with an AG-specific mouse monoclonal antibody (1:5000) (24) and an IRDye 680 anti-mouse IgG (1:2500) (Li-Cor).

Analysis of nuclear shape in fibroblasts

To assess nuclear shape abnormalities, early-passage mouse embryonic fibroblasts were grown on coverslips and then fixed and permeabilized (8). Cells were incubated with antibodies against lamin A (1:50, sc-20680, Santa Cruz Biotechnology) and prelamin A (1:50, clone 3C8) for 2 h. After washing, cells were incubated with Alexa Fluor 568-conjugated anti-rabbit antibody (1:500, Jackson ImmunoResearch Laboratories), Alexa Fluor 488-conjugated anti-rat antibody (1:500, Invitrogen) and DAPI to visualize DNA. Images were obtained on an Axiovert 200 MOT microscope (Zeiss) or on a Leica SP2 1P-FCS confocal microscope and nuclear shape was assessed (~1000 cells/genotype).

Analysis of nuclear stiffness in fibroblasts

Nuclear strain studies were performed as described previously (46), with the following modification. Cells were subjected to ~20% uniaxial strain rather than biaxial strain. Membrane and nuclear deformations were computed based on bright-field and fluorescent images acquired before, during and after strain application. Normalized nuclear strain was defined as the ratio of nuclear strain to membrane strain to compensate for small variations in applied membrane strain. Cells that were damaged during or after strain application were excluded from the analysis.

Immunohistochemistry

To assess the location of lamin A and prelamin A in tissues, 6–10-μm-thick frozen sections were prepared and placed on glass slides. The sections were fixed with cold (−20°C) methanol for 10 min, rinsed with acetone, permeabilized with 0.1% Tween in PBS, and then incubated in a PBS blocking buffer containing 0.1% Tween and 5% donkey serum for 1 h at room temperature. The sections were incubated with primary antibodies in blocking buffer overnight at a dilution

of 1:50 for a rabbit anti-lamin A antibody (Santa Cruz Biotechnology), 1:50 for a rat anti-prelamin A monoclonal antibody (3C8) and 1:50 for a rat anti-prelamin A antibody (7G11). Monoclonal antibodies 7G11 and 3C8 were derived from rats immunized with a C-terminal peptide of mouse prelamin A (34). After washing the sections, they were incubated for 1 h at room temperature with fluorescently labeled secondary antibodies (1:200 Alexa488-labeled anti-rat IgG; 1:200 Alexa568-labeled anti-rabbit IgG). The sections were then washed, post-fixed with 4% paraformaldehyde in PBS and stained with DAPI to visualize DNA. Images were obtained with an Axiovert 200 MOT microscope equipped with an Apotome and processed with AxoVision 4.2 software (Zeiss, Germany).

Analysis of mouse phenotypes

Body weights were measured weekly for 20 weeks and then every other week; numbers of surviving mice were recorded weekly. To assess osteolytic lesions and rib fractures, the thoracic cages of *Zmpste24*$^{-/-}$, *Lmna*$^{+/+}$, *Lmna*$^{PLAO/PLAO}$ and *Lmna*$^{nPLAO/nPLAO}$ mice were imaged by X-ray microtomography (μCT) with the Skyscan 1172 system (Skyscan).

Echocardiograms

Echocardiograms were obtained on *Lmna*$^{+/+}$, *Lmna*$^{PLAO/PLAO}$ and *Lmna*$^{nPLAO/nPLAO}$ mice anesthetized with 2% isoflurane with the Vevo 770 Imaging system and 35 mHz scan probe (Visualsonics). Data were analyzed using the Vevo analysis program. LV chamber diameters during systole (LV Vol:s) and diastole (LV Vol:d) were measured from *M*-mode recordings. LV ejection fraction (%) was calculated as [(LV Vol:d − LV Vol:s)/LV Vol:d] × 100.

Histology

To assess fibrosis, *Lmna*$^{+/+}$ and *Lmna*$^{nPLAO/nPLAO}$ mice were perfused with 4% paraformaldehyde, and the hearts were removed and post-fixed in 3% formalin. Fixed tissues were embedded in paraffin, sectioned and stained with Gomori trichrome and hematoxylin.

Quantitative reverse transcribed–PCR

Total RNA was prepared from mouse hearts with the RNeasy kit (Qiagen). RNA was treated with DNase I (Ambion) and reverse transcribed (RT) with a mixture of random primers, oligo(dT) and Superscript III (Invitrogen). Primers 5′-CGCA TCAAGGAGCTCACC-3′ and 5′-CCTGCAGCCGCATTA AGT-3′ were used to amplify the mouse *Myh6* cDNA, and primers 5′-GGAAGACAGGAAGAACCTACTGC-3′ and 5′-AA CTTGGACAGGTTGGTGTTG-3′ were used to amplify mouse *Myh7* cDNA. Expression was normalized to GAPDH (amplified with the primers 5′- GCACAGTCAAGGCCGAGAAT-3′ and 5′-GCCTTCTCCATGGTGGTGAA-3′). PCRs were performed in triplicate on a 7900HT Fast Real-Time PCR system (Applied Biosystems, Foster City, CA, USA). Gene-expression levels were calculated with the comparative cycle threshold (C_T) method.

Statistical analyses

Differences in misshapen nuclei were analyzed using the χ^2 test. Variations in nuclear strain assays were analyzed by one-way ANOVA with Tukey's multiple comparison post-test. The number of surviving male and female mice was recorded weekly. Differences were assessed by the log-rank (Mantel–Cox) and the Gehan–Breslow–Wilcoxon tests. Body weight curves were compared with repeated-measures ANOVA. Echocardiographic data and gene-expression data were analyzed with the Student's *t*-test.

ACKNOWLEDGEMENT

We thank Dr David Frost from Abbott Pharmaceuticals for ABT-100.

Conflict of Interest statement. None declared.

FUNDING

This work was supported by the National Institutes of Health (HL76839, HL86683, HL089781, GM66152, AG035626, HL082792, NS059348); a March of Dimes Grant (6-FY2007-1012); the Ellison Medical Foundation Senior Scholar Program; a post-doctoral fellowship award from the American Heart Association, Western States Affiliate; and a Scientist Development Grant from the American Heart Association (0635359N).

REFERENCES

1. Casey, P.J. (1992) Biochemistry of protein prenylation. *J. Lipid Res.*, **33**, 1731–1740.
2. Casey, P.J. and Seabra, M.C. (1996) Protein prenyltransferases. *J. Biol. Chem.*, **271**, 5289–5292.
3. Clarke, S. (1992) Protein isoprenylation and methylation at carboxyl-terminal cysteine residues. *Annu. Rev. Biochem.*, **61**, 355–386.
4. Davies, B.S., Fong, L.G., Yang, S.H., Coffinier, C. and Young, S.G. (2009) The posttranslational processing of prelamin A and disease. *Annu. Rev. Genomics Hum. Genet.*, **10**, 153–174.
5. Sinensky, M., Fantle, K., Trujillo, M., McLain, T., Kupfer, A. and Dalton, M. (1994) The processing pathway of prelamin A. *J. Cell Sci.*, **107**, 61–67.
6. Bergo, M.O., Gavino, B., Ross, J., Schmidt, W.K., Hong, C., Kendall, L.V., Mohr, A., Meta, M., Genant, H., Jiang, Y. *et al.* (2002) Zmpste24 deficiency in mice causes spontaneous bone fractures, muscle weakness, and a prelamin A processing defect. *Proc. Natl Acad. Sci. USA*, **99**, 13049–13054.
7. Corrigan, D.P., Kuszczak, D., Rusinol, A.E., Thewke, D.P., Hrycyna, C.A., Michaelis, S. and Sinensky, M.S. (2005) Prelamin A endoproteolytic processing *in vitro* by recombinant Zmpste24. *Biochem. J.*, **387**, 129–138.
8. Fong, L.G., Ng, J.K., Meta, M., CotÇ, N., Yang, S.H., Stewart, C.L., Sullivan, T., Burghardt, A., Majumdar, S., Reue, K. *et al.* (2004) Heterozygosity for Lmna deficiency eliminates the progeria-like phenotypes in Zmpste24-deficient mice. *Proc. Natl Acad. Sci. USA*, **101**, 18111–18116.
9. Pendas, A.M., Zhou, Z., Cadinanos, J., Freije, J.M.P., Wang, J., Hultenby, K., Astudillo, A., Wernerson, A., Rodriguez, F., Tryggvason, K. *et al.* (2002) Defective prelamin A processing and muscular and adipocyte alterations in Zmpste24 metalloproteinase-deficient mice. *Nat. Genet.*, **31**, 94–99.
10. Eriksson, M., Brown, W.T., Gordon, L.B., Glynn, M.W., Singer, J., Scott, L., Erdos, M.R., Robbins, C.M., Moses, T.Y., Berglund, P. *et al.* (2003)

Recurrent *de novo* point mutations in lamin A cause Hutchinson–Gilford progeria syndrome. *Nature*, **423**, 293–298.
11. Dechat, T., Shimi, T., Adam, S.A., Rusinol, A.E., Andres, D.A., Spielmann, H.P., Sinensky, M.S. and Goldman, R.D. (2007) Alterations in mitosis and cell cycle progression caused by a mutant lamin A known to accelerate human aging. *Proc. Natl Acad. Sci. USA*, **104**, 4955–4960.
12. Yang, S.H., Andres, D.A., Spielmann, H.P., Young, S.G. and Fong, L.G. (2008) Progerin elicits disease phenotypes of progeria in mice whether or not it is farnesylated. *J. Clin. Invest.*, **118**, 3291–3300.
13. De Sandre-Giovannoli, A., Bernard, R., Cau, P., Navarro, C., Amiel, J., Boccaccio, I., Lyonnet, S., Stewart, C.L., Munnich, A., Le Merrer, M. *et al.* (2003) Lamin A truncation in Hutchinson–Gilford progeria. *Science*, **300**, 2055.
14. Capell, B.C., Erdos, M.R., Madigan, J.P., Fiordalisi, J.J., Varga, R., Conneely, K.N., Gordon, L.B., Der, C.J., Cox, A.D. and Collins, F.S. (2005) Inhibiting farnesylation of progerin prevents the characteristic nuclear blebbing of Hutchinson–Gilford progeria syndrome. *Proc. Natl Acad. Sci. USA*, **102**, 12879–12884.
15. Glynn, M.W. and Glover, T.W. (2005) Incomplete processing of mutant lamin A in Hutchinson–Gilford progeria leads to nuclear abnormalities, which are reversed by farnesyltransferase inhibition. *Hum. Mol. Genet.*, **14**, 2959–2969.
16. Mallampalli, M.P., Huyer, G., Bendale, P., Gelb, M.H. and Michaelis, S. (2005) Inhibiting farnesylation reverses the nuclear morphology defect in a HeLa cell model for Hutchinson–Gilford progeria syndrome. *Proc. Natl Acad. Sci. USA*, **102**, 14416–14421.
17. Toth, J.I., Yang, S.H., Qiao, X., Beigneux, A.P., Gelb, M.H., Moulson, C.L., Miner, J.H., Young, S.G. and Fong, L.G. (2005) Blocking protein farnesyltransferase improves nuclear shape in fibroblasts from humans with progeroid syndromes. *Proc. Natl Acad. Sci. USA*, **102**, 12873–12878.
18. Yang, S.H., Bergo, M.O., Toth, J.I., Qiao, X., Hu, Y., Sandoval, S., Meta, M., Bendale, P., Gelb, M.H., Young, S.G. *et al.* (2005) Blocking protein farnesyltransferase improves nuclear blebbing in mouse fibroblasts with a targeted Hutchinson–Gilford progeria syndrome mutation. *Proc. Natl Acad. Sci. USA*, **102**, 10291–10296.
19. Yang, S.H., Meta, M., Qiao, X., Frost, D., Bauch, J., Coffinier, C., Majumdar, S., Bergo, M.O., Young, S.G. and Fong, L.G. (2006) A farnesyltransferase inhibitor improves disease phenotypes in mice with a Hutchinson–Gilford progeria syndrome mutation. *J. Clin. Invest.*, **116**, 2115–2121.
20. Yang, S.H., Chang, S.Y., Andres, D.A., Spielmann, H.P., Young, S.G. and Fong, L.G. (2010) Assessing the efficacy of protein farnesyltransferase inhibitors in mouse models of progeria. *J. Lipid Res.*, **51**, 400–405.
21. Yang, S.H., Qiao, X., Fong, L.G. and Young, S.G. (2008) Treatment with a farnesyltransferase inhibitor improves survival in mice with a Hutchinson–Gilford progeria syndrome mutation. *Biochim. Biophys. Acta*, **1781**, 36–39.
22. Kieran, M.W., Gordon, L. and Kleinman, M. (2007) New approaches to progeria. *Pediatrics*, **120**, 834–841.
23. Verstraeten, V.L.R.M., Broers, J.L.V., van Steensel, M.A.M., Zinn-Justin, S., Ramaekers, F.C.S., Steijlen, P.M., Kamps, M., Kuijpers, H.J.H., Merckx, D., Smeets, H.J.M. *et al.* (2006) Compound heterozygosity for mutations in LMNA causes a progeria syndrome without prelamin A accumulation. *Hum. Mol. Genet.*, **15**, 2509–2522.
24. Troutman, J.M., Roberts, M.J., Andres, D.A. and Spielmann, H.P. (2005) Tools to analyze protein farnesylation in cells. *Bioconjug. Chem.*, **16**, 1209–1217.
25. Lowes, B.D., Minobe, W., Abraham, W.T., Rizeq, M.N., Bohlmeyer, T.J., Quaife, R.A., Roden, R.L., Dutcher, D.L., Robertson, A.D., Voelkel, N.F. *et al.* (1997) Changes in gene expression in the intact human heart. Downregulation of alpha-myosin heavy chain in hypertrophied, failing ventricular myocardium. *J. Clin. Invest.*, **100**, 2315–2324.
26. Arimura, T., Helbling-Leclerc, A., Massart, C., Varnous, S., Niel, F., Lacene, E., Fromes, Y., Toussaint, M., Mura, A.M., Keller, D.I. *et al.* (2005) Mouse model carrying H222P-Lmna mutation develops muscular dystrophy and dilated cardiomyopathy similar to human striated muscle laminopathies. *Hum. Mol. Genet.*, **14**, 155–169.
27. DeBusk, F.L. (1972) The Hutchinson–Gilford progeria syndrome. Report of 4 cases and review of the literature. *J. Pediatr.*, **80**, 697–724.
28. Fernandez-Palazzi, F., McLaren, A.T. and Slowie, D.F. (1992) Report on a case of Hutchinson–Gilford progeria, with special reference to orthopedic problems. *Eur. J. Pediatr. Surg.*, **2**, 378–382.
29. Bonne, G., Barletta, M.R.D., Varnous, S., Becane, H.-M., Hammouda, E.-H., Merlini, L., Muntoni, F., Greenberg, C.R., Gary, F., Urtizberea, J.-A. *et al.* (1999) Mutations in the gene encoding lamin A/C cause autosomal dominant Emery-Dreifuss muscular dystrophy. *Nat. Genet.*, **21**, 285–288.
30. Muchir, A., Bonne, G., van der Kooi, A.J., van Meegen, M., Baas, F., Bolhuis, P.A., de Visser, M. and Schwartz, K. (2000) Identification of mutations in the gene encoding lamins A/C in autosomal dominant limb girdle muscular dystrophy with atrioventricular conduction disturbances (LGMD1B). *Hum. Mol. Genet.*, **9**, 1453–1459.
31. Vytopil, M., Benedetti, S., Ricci, E., Galluzzi, G., Dello Russo, A., Merlini, L., Boriani, G., Gallina, M., Morandi, L., Politano, L. *et al.* (2003) Mutation analysis of the lamin A/C gene (LMNA) among patients with different cardiomuscular phenotypes. *J. Med. Genet.*, **40**, e132–e132.
32. Mounkes, L.C., Kozlov, S.V., Rottman, J.N. and Stewart, C.L. (2005) Expression of an LMNA-N195K variant of A-type lamins results in cardiac conduction defects and death in mice. *Hum. Mol. Genet.*, **14**, 2167–2180.
33. Muchir, A., Pavlidis, P., Decostre, V., Herron, A.J., Arimura, T., Bonne, G. and Worman, H.J. (2007) Activation of MAPK pathways links LMNA mutations to cardiomyopathy in Emery-Dreifuss muscular dystrophy. *J. Clin. Invest.*, **117**, 1282–1293.
34. Lee, R., Chang, S.Y., Trinh, H., Tu, Y., White, A.C., Davies, B.S., Bergo, M.O., Fong, L.G., Lowry, W.E. and Young, S.G. (2010) Genetic studies on the functional relevance of the protein prenyltransferases in skin keratinocytes. *Hum. Mol. Genet.*, **19**, 1603–1617.
35. Maurer-Stroh, S., Koranda, M., Benetka, W., Schneider, G., Sirota, F.L. and Eisenhaber, F. (2007) Towards complete sets of farnesylated and geranylgeranylated proteins. *PLoS Comput. Biol.*, **3**, e66.
36. Reid, T.S., Terry, K.L., Casey, P.J. and Beese, L.S. (2004) Crystallographic analysis of CaaX prenyltransferases complexed with substrates defines rules of protein substrate selectivity. *J. Mol. Biol.*, **343**, 417–433.
37. Mijimolle, N., Velasco, J., Dubus, P., Guerra, C., Weinbaum, C.A., Casey, P.J., Campuzano, V. and Barbacid, M. (2005) Protein farnesyltransferase in embryogenesis, adult homeostasis, and tumor development. *Cancer Cell*, **7**, 313–324.
38. Fong, L.G., Ng, J.K., Lammerding, J., Vickers, T.A., Meta, M., CotÇ, N., Gavino, B., Qiao, X., Chang, S.Y., Young, S.R. *et al.* (2006) Prelamin A and lamin A appear to be dispensable in the nuclear lamina. *J. Clin. Invest.*, **116**, 632–634.
39. Sullivan, T., Escalante-Alcalde, D., Bhatt, H., Anver, M., Bhat, N., Nagashima, K., Stewart, C.L. and Burke, B. (1999) Loss of A-type lamin expression compromises nuclear envelope integrity leading to muscular dystrophy. *J. Cell Biol.*, **147**, 913–920.
40. Beck, L.A., Hosick, T.J. and Sinensky, M. (1988) Incorporation of a product of mevalonic acid metabolism into proteins of Chinese hamster ovary cell nuclei. *J. Cell Biol.*, **107**, 1307–1316.
41. Lutz, R.J., Trujillo, M.A., Denham, K.S., Wenger, L. and Sinensky, M. (1992) Nucleoplasmic localization of prelamin A: implications for prenylation-dependent lamin A assembly into the nuclear lamina. *Proc. Natl Acad. Sci. USA*, **89**, 3000–3004.
42. Hennekes, H. and Nigg, E.A. (1994) The role of isoprenylation in membrane attachment of nuclear lamins. A single point mutation prevents proteolytic cleavage of the lamin A precursor and confers membrane binding properties. *J. Cell Sci.*, **107**, 1019–1029.
43. Fong, L.G., Frost, D., Meta, M., Qiao, X., Yang, S.H., Coffinier, C. and Young, S.G. (2006) A protein farnesyltransferase inhibitor ameliorates disease in a mouse model of progeria. *Science*, **311**, 1621–1623.
44. Leung, G.K., Schmidt, W.K., Bergo, M.O., Gavino, B., Wong, D.H., Tam, A., Ashby, M.N., Michaelis, S. and Young, S.G. (2001) Biochemical studies of Zmpste24-deficient mice. *J. Biol. Chem.*, **276**, 29051–29058.
45. Dalton, M. and Sinensky, M. (1995) Expression systems for nuclear lamin proteins: farnesylation in assembly of nuclear lamina. In Patrick, J.C. and Janice, E.B. (eds), *Methods in Enzymology*. Academic Press, San Diego, CA, USA, Vol. **250**, pp. 134–148.
46. Lammerding, J., Fong, L.G., Ji, J.Y., Reue, K., Stewart, C.L., Young, S.G. and Lee, R.T. (2006) Lamins A and C but not lamin B1 regulate nuclear mechanics. *J. Biol. Chem.*, **281**, 25768–25780.